LETTER

doi:10.1038/nature09880

Functional specificity of local synaptic connections in neocortical networks

Ho Ko[1]*, Sonja B. Hofer[1]*, Bruno Pichler[1]†, Katherine A. Buchanan[1], P. Jesper Sjöström[1] & Thomas D. Mrsic-Flogel[1]

Neuronal connectivity is fundamental to information processing in the brain. Therefore, understanding the mechanisms of sensory processing requires uncovering how connection patterns between neurons relate to their function. On a coarse scale, long-range projections can preferentially link cortical regions with similar responses to sensory stimuli[1–4]. But on the local scale, where dendrites and axons overlap substantially, the functional specificity of connections remains unknown. Here we determine synaptic connectivity between nearby layer 2/3 pyramidal neurons *in vitro*, the response properties of which were first characterized in mouse visual cortex *in vivo*. We found that connection probability was related to the similarity of visually driven neuronal activity. Neurons with the same preference for oriented stimuli connected at twice the rate of neurons with orthogonal orientation preferences. Neurons responding similarly to naturalistic stimuli formed connections at much higher rates than those with uncorrelated responses. Bidirectional synaptic connections were found more frequently between neuronal pairs with strongly correlated visual responses. Our results reveal the degree of functional specificity of local synaptic connections in the visual cortex, and point to the existence of fine-scale subnetworks dedicated to processing related sensory information.

Paired intracellular recordings in cortical slices indicate that synaptic connectivity between neighbouring neurons is heterogeneous and depends on factors such as cell type, electrophysiological properties and long-range targets[5–10]. In fact, even within relatively homogenous groups of neurons, connectivity is not uniformly distributed[5,6]. Although this non-random connectivity raises the possibility that functionally similar neurons form synaptically coupled subnetworks[6,7], the relationship between a neuron's synaptic partners and their functional properties in local cortical circuits has not been determined.

To elucidate this relationship, we developed an approach to relate connectivity to function in identified neurons of the layer 2/3 (L2/3) network in mouse visual cortex (V1), where neurons with diverse preferences for sensory stimuli are locally intermixed[11,12]. In anaesthetized mice, the monocular region of V1 was bulk labelled with injections of the calcium indicator dye OGB-1 AM and the astrocyte marker SR101 (ref. 13) (see Methods). We first used *in vivo* two-photon imaging[14,15] to sample spike-related somatic calcium signals from L2/3 neurons during presentation of drifting gratings and natural movie sequences (see Methods). We repeated this mapping at consecutive depths beneath the cortical surface to characterize visually evoked responses of all neurons within a cortical volume of approximately $285 \times 285 \times 90$ μm^3, starting at the upper border of L2/3 (Fig. 1a, b; depth range covered 60–120 μm). In this way, we obtained information about orientation/direction tuning and response correlation from a complete sample of L2/3 neurons (Fig. 1c, d).

We then identified the same OGB-1-filled neurons in acute slices (Figs 1e–h, 2a) by registering image stacks obtained *in vivo* and *in vitro* using affine transformation (see Methods and Supplementary Fig. 1), and carried out simultaneous whole-cell patch-clamp recordings from up to four neighbouring L2/3 pyramidal neurons (mean distance ± standard deviation (s.d.) = 25 ± 9 μm). Synaptic connectivity

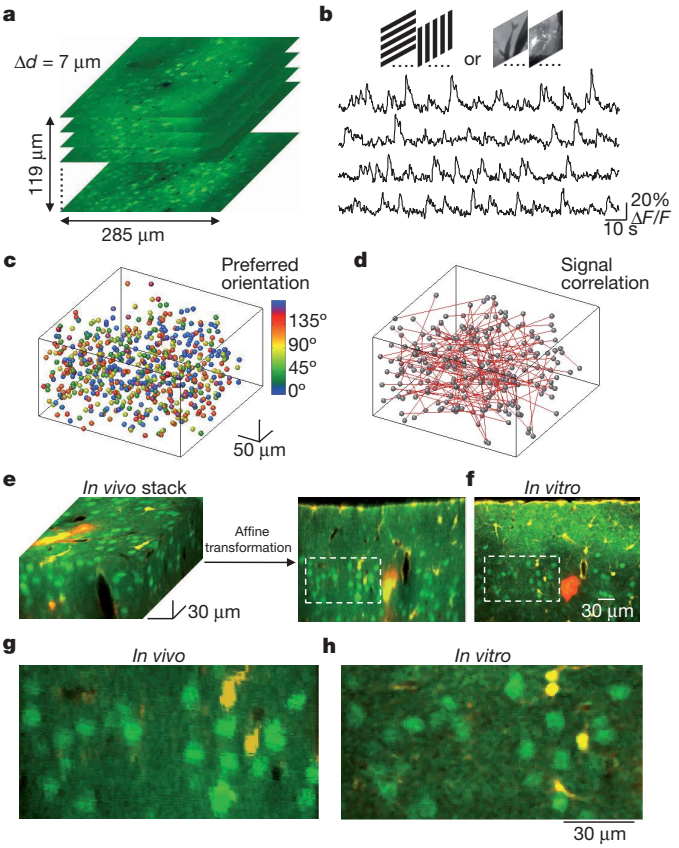

Figure 1 | Imaging functional properties of neurons *in vivo* and indentifying the same neurons *in vitro*. **a**, Two-photon imaging was used to sample somatic calcium signals from a complete population of L2/3 neurons within a $285 \times 285 \times 119$ μm^3 volume. Imaging was carried out at 7 μm depth increments ($\Delta d = 7$ μm). Neurons were labelled with the calcium indicator dye OGB-1 AM (green) and the astrocyte marker SR101 (red). **b**, Example traces of calcium signals from four different cells in the imaged volume while presenting six trials of grating stimuli drifting in eight different directions. **c**, All orientation-selective cells in the volume were colour-coded according to preferred orientation and plotted as spheres. **d**, Signal correlations were computed from average responses to natural movies. Red lines represent strongly correlated neuronal pairs (signal correlation >0.2). **e**, **f**, After imaging visually evoked calcium signals, a detailed image stack was obtained *in vivo*. The brain was sliced coronally and another stack of the same tissue was obtained *in vitro* (a single optical plane is shown in **f**). Affine transformation was used to align the *in vivo* to the *in vitro* stack, allowing precise matching of OGB-1-filled cells in the two stacks. **g**, **h**, Close-ups of the regions outlined with dashed lines in **e** and **f**, respectively.

[1]Department of Neuroscience, Physiology and Pharmacology, University College London, 21 University Street, London WC1E 6DE, UK. †Present address: MRC National Institute for Medical Research, The Ridgeway, Mill Hill, London NW7 1AA, UK.
*These authors contributed equally to this work.

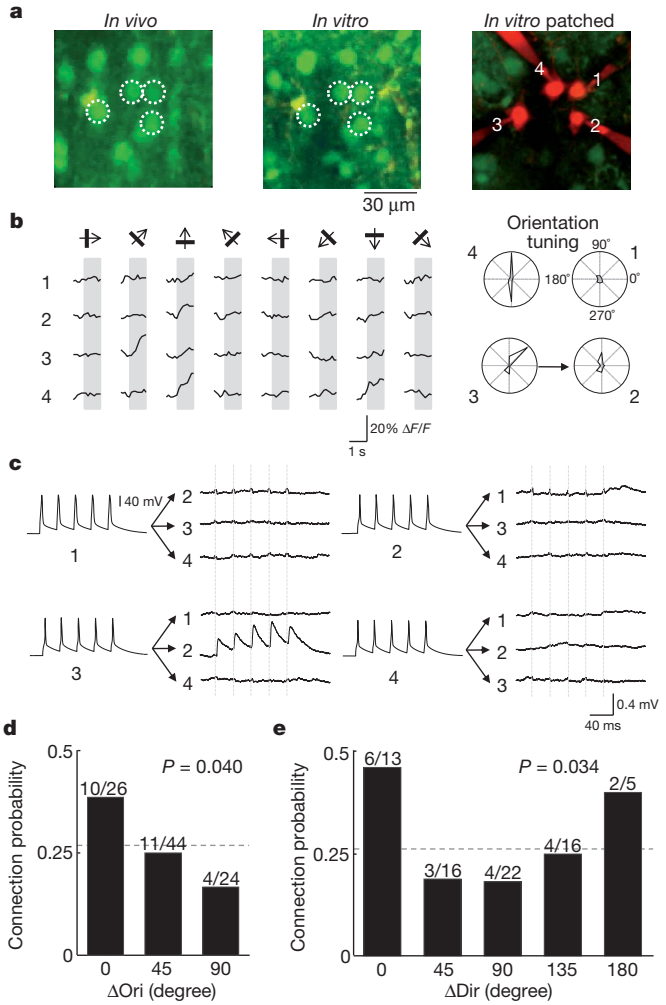

Figure 2 | Relating orientation and direction preference to connection probability among L2/3 pyramidal neurons. **a**, White circles denote the locations of *in vivo* to *in vitro* matched cells that were targeted for whole-cell recording and filled with Alexa 594. **b**, Left panel shows average calcium responses of the four cells to oriented drifting gratings. Right panel shows corresponding polar plots of inferred spike rate responses, normalized to the maximum response of cell 4. Three of the cells (cells 2, 3 and 4) were reliably responsive and orientation selective. Arrow shows a connection detected from cell 3 to cell 2. **c**, Membrane potential recordings from the four cells. Currents were injected into each cell in sequence, and from average traces of postsynaptic potentials an excitatory connection was found from cell 3 to cell 2. No other connections were found. Vertical dashed lines indicate timing of presynaptic spikes. In some traces, stimulation artefacts are visible that coincided exactly with presynaptic spikes and therefore could be clearly distinguished from EPSPs. **d**, Relationship between connection probability and difference in preferred orientation (ΔOri) among pairs in which both neurons were responsive to grating stimuli and were orientation selective (OSI >0.4). There was a significant decreasing trend in connection probability as ΔOri increased ($P = 0.040$, Cochran–Armitage test). Dotted line indicates connection probability for all pairs included in this analysis (25/94, 0.27). The bins include difference in orientation values of 0 to 22.5° (0 degree bin), 22.5° to 67.5° (45 degree bin), and 67.5° to 90° (90 degree bin). **e**, Relationship between connection probability and difference in preferred direction (ΔDir) in the subset of neurons that were direction-selective (DSI >0.3). The same decreasing trend with respect to ΔOri was detected ($P = 0.034$, Cochran–Armitage test). Neurons connected with specificity to preferred orientation but not to preferred direction. Dotted line indicates connection probability for all directionally selective pairs (19/72, 0.26). The bins include difference in orientation values of 0 to 22.5° (0 degree bin), 22.5° to 67.5° (45 degree bin), and so on.

between cells was assessed by evoking action potentials in each neuron in turn while simultaneously recording membrane potential in the other neurons. Monosynaptic connections appeared as spike-locked postsynaptic potentials with millisecond latency (mean latency ± s.e.m. = 1.69 ± 0.11 ms; see Figs 2c, 3b for sample traces). This approach allowed us to determine connectivity rates and patterns (unidirectional, bidirectional), and to relate these to cell functionality in the intact brain (Figs 1c, d, 2b, 3a).

The data set contained imaging experiments performed on 16 mice and whole-cell recordings from 126 L2/3 pyramidal cells, 116 of which could be matched to neurons functionally characterized *in vivo* (see Methods). The rate of connectivity was 0.19 (43 connections out of 222 potential connections assayed), in keeping with previous reports[6,10]. Connection probability, synaptic strength and electrophysiological properties of OGB-1-labelled neurons were not significantly different to those recorded in slices from naive age-matched visual cortex that was not injected with OGB-1 AM (connectivity rate 0.18; 25 connected of 143 tested; Supplementary Fig. 2), indicating that dye loading, anaesthesia and prolonged exposure to infrared laser light during imaging *in vivo* did not alter these parameters.

We first examined how connectivity depended on orientation selectivity and on responsiveness to natural movies. Out of the 116 neurons, 77 were responsive to the natural movie, and 79 were orientation selective for grating stimuli (see Methods). Connection probability between orientation-tuned neurons was more than twofold higher than among non-selective and/or non-responsive cells (0.27; 25/94 versus 0.10; 3/31; $P = 0.050$, chi-squared test). The connectivity rate between neurons responsive to the natural movie was significantly higher than among cells non-responsive to the movie (0.28; 30/108 versus 0.04; 2/48; $P = 0.001$, chi-squared test). Taken together, these data indicate that reliably responsive and feature-selective neurons belong to more densely interconnected neocortical subnetworks.

We then related connection probability to neuronal preference for the angle and direction of drifting gratings (Fig. 2). For this analysis, we only included pairs in which both neurons were responsive (74/113), orientation selective (orientation selectivity index (OSI) >0.4; 53/74), or direction selective (direction selectivity index (DSI) >0.3; 41/53; see Methods and Supplementary Fig. 3a–c). Connectivity rate decreased with increasing difference in orientation preference ($P = 0.040$, Cochran–Armitage test for trend; Fig. 2d). For similarly tuned cells,

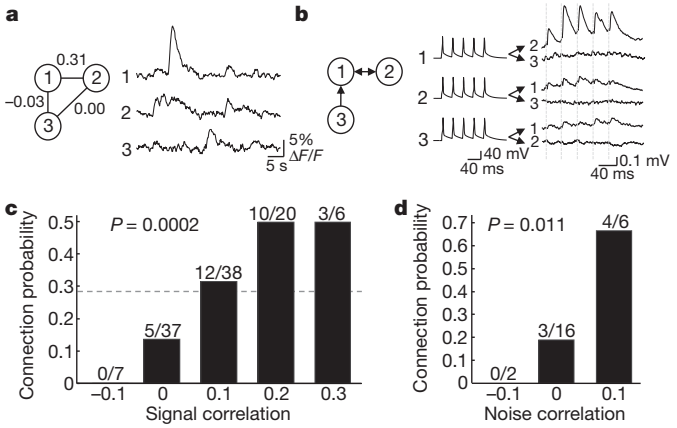

Figure 3 | Relationship between response correlation to natural movies and connection probability. **a**, An example of a triplet of neurons targeted for whole-cell recording *in vitro*, with associated *in vivo* calcium responses to the natural movie (average of six repetitions) and spike rate correlation values. Neuron 1 and 2 showed correlated firing (signal correlation = 0.31), whereas other pairs did not. **b**, Triple recordings from the same neurons reveal the pattern of connections: neurons 1 and 2 were bidirectionally connected, whereas neuron 3 provided input to neuron 1. Dashed lines indicate timing of presynaptic spikes. **c**, There was a significant increase in connection probability with increasing signal correlation to natural movies ($P = 0.0002$, Cochran–Armitage test). Dotted line indicates connection probability for all pairs included in this analysis (30/108, 0.28). **d**, Connection probability increased significantly with increase in noise correlation ($P = 0.011$, Cochran–Armitage test). Correlation values were binned, with ranges from −0.15 to −0.05, from −0.05 to 0.05, and so on.

connection probability was high (0.38; 10/26; difference in preferred orientation (ΔOri) <22.5°), more than twofold higher than for cells with a large difference in orientation preference (0.17; 4/24; ΔOri >67.5°). Thus, neuronal pairs similarly tuned for orientation were more likely to connect to each other, although a considerable connectivity rate was still observed between neurons tuned to dissimilar or orthogonal orientations. These results are consistent with the narrow suprathreshold yet broader subthreshold tuning for orientation and direction in mouse V1 neurons[16]. The same decrease of connection probability with increase in ΔOri was found for direction selective pairs ($P = 0.034$, Cochran–Armitage test; Fig. 2e), but these neurons only connected specifically with respect to orientation not preferred direction (Fig. 2e). These data indicate that directional preference is not conferred by biased local excitatory input, so other cell intrinsic or network mechanisms (for example, biased long range input, specific inhibition) may be needed to explain the emergence of direction selectivity. Varying the criteria for orientation or direction selectivity (OSI/DSI from 0.2 to 0.6) did not change the dependence of connectivity on difference in orientation/direction preference (Supplementary Fig. 3d, e), indicating that neurons that are broadly or sharply tuned both tend to connect preferentially to others with similar functional preference. In our data set we did not find evidence indicating that neurons with similar preferred orientations or directions are connected by stronger (excitatory postsynaptic potential (EPSP) amplitude) or more facilitating (paired-pulse ratio (PPR)) connections than neurons with different preferred orientations or directions (Supplementary Fig. 4a, b, d, e; also see Supplementary Fig. 5 for a sample pair with strong connections), although the sample size may not be adequate for ruling out any subtle trends.

The visual cortical circuit is constantly engaged in processing natural scenes, so statistical dependencies between neuronal activities in the presence of such stimuli may reflect connectivity. We therefore tested how network connectivity relates to the similarity of neuronal responses during the presentation of stimuli with natural spatiotemporal statistics (Fig. 3, see Methods). For each neuronal pair in which both neurons responded reliably to natural movies (56/113), we computed the time-varying firing-rate correlation of average responses (signal correlation) to repeated presentations of a 30 to 40-s-long natural movie sequence (Fig. 3a). On average, signal correlations were low (mean ± s.d. = 0.08 ± 0.10). The probability of finding a connection between two neurons significantly increased with signal correlation to natural movies ($P = 0.0002$, Cochran–Armitage test; Fig. 3c). For pairs with close to zero or weakly negative signal correlation (<0.05), the connection probability was low (0.11, 5/44). In contrast, for neuronal pairs with stronger signal correlation (>0.15), the connection probability was more than fourfold higher (0.5; 13/26). Therefore, connectivity in mouse visual cortex is highly selective with respect to neuronal responses to natural movies. EPSP amplitude and PPR, however, were not found to change significantly with increase in signal correlation (Supplementary Fig. 4c, f; also see Supplementary Fig. 5), although the sample size may not be large enough to rule out subtle trends.

Correlated variability in neuronal firing independent of a sensory stimulus is assumed to reflect neuronal connectivity in the network[17–19]. Correlated fluctuations in neuronal firing may either be driven by common input or by recurrent synaptic connections, or both. For a subset of visually responsive neuronal pairs (12/56) that were imaged simultaneously *in vivo* (that is, on the same optical planes), we computed noise correlations (see Methods), which provide an indication of correlated response variability. Noise correlations were low (mean ± s.d. = 0.02 ± 0.04). Despite the small sample size, connection probability was found to increase significantly with increase in noise correlation (Fig. 3d; $P = 0.011$, Cochran–Armitage test), indicating that recurrent connectivity may contribute to correlated fluctuations of neuronal firing.

We next compared how visual response similarity relates to connectivity motifs in the local network. Previous work indicates that bidirectional connections are overrepresented in a network of sparsely connected pyramidal neurons[5]. We found that the connectivity bias between neurons responding similarly to drifting gratings or to natural movies was further accentuated when investigating the distribution of unidirectionally or bidirectionally connected pairs (Fig. 4). We found a decreasing trend relating probability of bidirectional connections and difference in orientation preference (Fig. 4a, b; $P = 0.070$ for all orientation-selective pairs; $P = 0.036$ for direction-selective pairs, Cochran–Armitage test). Importantly, the monotonic fall-off in the incidence of bidirectional motifs was steeper than the overall decrease in probability of finding connected pairs as ΔOri increased (Fig. 4a, b). Similarly, the incidence of bidirectional connections increased sharply as signal correlation to natural movies increased ($P = 0.003$, Cochran–Armitage test; Fig. 4c), such that signal correlation was almost threefold higher for recurrently connected pairs than unconnected pairs (mean signal correlation of bidirectionally connected pairs ± s.d. = 0.16 ± 0.07 versus 0.06 ± 0.10 for unconnected pairs; $P = 0.01$, rank sum test). As the probability of unidirectionally connected pairs did not show a monotonic trend with increase in response similarity (Fig. 4a–c; $P > 0.4$ for all conditions, Cochran–Armitage test), reciprocal connectivity reflects functional similarity better than does unidirectional connectivity.

In this study, we have characterized the functional specificity of local connections in mouse V1. Our results demonstrate that connectivity between neighbouring neurons (<50 μm apart) is not random, but specifically structured; visually driven neurons were more likely to connect to each other, and this probability increased with the degree of their response similarity. This relationship between connectivity and function was stronger when comparing responses to natural sensory input than for relatively artificial grating stimuli.

We have shown in mouse V1 that—although a given neuron receives input from nearby neurons preferring a wide range of stimulus

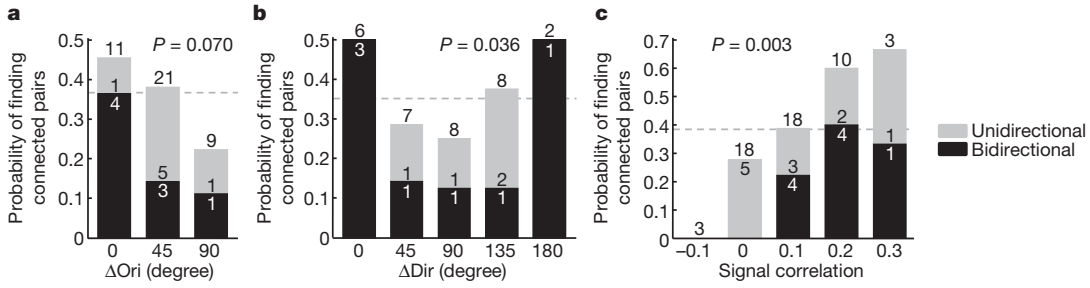

Figure 4 | Relationship between similarity of visual responses and probability of finding unidirectionally and bidirectionally connected pairs. **a**, Among orientation-selective neurons, the probability of finding connected pairs decreased as ΔOri increased. The fall-off in probability of finding bidirectionally connected pairs was steeper than the decrease in overall probability of finding connected pairs. A trend of decrease in probability of finding bidirectionally connected pairs was found ($P = 0.070$, Cochran–Armitage test). **b**, The same observation holds in the subset of directionally selective pairs, and the probability of finding bidirectionally connected pairs decreased as ΔOri increased ($P = 0.036$, Cochran–Armitage test). **c**, The probability of finding bidirectionally connected pairs increased sharply as signal correlation to natural movies increased ($P = 0.003$, Cochran–Armitage test). Dotted lines indicate the probability of finding connected pairs from all pairs included in analysis (panel **a**: 15/41, 0.37; panel **b**: 11/31, 0.35; panel **c**: 20/52, 0.38).

orientations—more than twice as many connections are made between similarly tuned neurons as between disparately tuned cells. In keeping, subthreshold tuning in L2/3 pyramidal neurons in mouse V1 is broad but nonetheless biased towards the preferred orientation[16]. This is similar to the tuning of neurons in pinwheel centres of orientation maps in visual cortex of other species[20]. In carnivores and primates, long-range horizontal projections in L2/3 (>500 μm) are biased towards cortical columns with similar orientation preference[1–4]. Our results indicate that similar principles of connectivity apply at the level of local neocortical networks in the mouse—a species without columnar architecture—indicating that functionally biased connectivity may be a general feature of organization in the visual cortex. In the visual cortex this selective connection scheme may serve as a mechanism for the amplification of thalamic input and sharpening of tuning[21,22] or for local contour integration[23].

Analysis of connectivity rate with respect to similarity of responses to natural movies revealed a marked degree of specificity of local connections (Fig. 3c, d). Connection probability increased sharply with increase in both signal and noise correlation to natural movies. Neurons with higher signal correlations to natural movies probably share similar receptive field structures, and may therefore be driven by common feed-forward input[24]. Our results are therefore consistent with the finding that L2/3 pyramidal neurons form highly interconnected subnetworks sharing common input from layer 4 in slices of rat visual cortex[6]. Developmentally, this organization of lateral connections based on receptive field similarity may arise through activity-dependent synaptic plasticity, whereby neurons driven by common input develop stable bidirectional connections[25]. Indeed, our data show that the majority of bidirectionally connected neurons had stronger signal correlations to natural movies and shared similar orientation preference. As individual neurons show variability in their responses to the same visual stimulus[26], recurrent excitation between similarly tuned neurons may reduce response variance, while introducing redundancy into the population code for robustness against errors[27].

Our results do not preclude the possibility that other factors—including inhibitory connections or synaptic strength—also contribute to functional specificity in the circuit. Because inhibition, in particular, may be important in determining the receptive field properties of neurons in V1 (ref. 28), it will be important to examine the extent to which inhibitory connections are functionally specific[7].

Using a novel and relatively straightforward approach for *in vitro* mapping of synaptic connectivity among neurons that had been identified functionally *in vivo*, we found that neighbouring neurons with similar feature selectivity preferentially but not exclusively connected to each other in L2/3 of mouse V1. Together with other powerful approaches[29,30], our method can be used to uncover functional biases of connectivity between different cell types and cortical layers, and in other brain areas. This information will be critical for understanding the functional wiring of circuits mediating perception and behaviour.

METHODS SUMMARY

Anaesthetized C57Bl/6 mice between postnatal day 22 and 26 were injected with the calcium-sensitive dye Oregon Green Bapta-1 AM into monocular V1 as described previously[11] and *in vivo* two-photon calcium imaging[14,15] was used to record responses of layer 2/3 neurons to eight different drifting square-wave gratings (0.035 cycles per degree, 2 cycles s^{-1}, 100% contrast) and natural movie sequences. Spike trains were inferred from calcium signals using a non-negative deconvolution method. Preferred orientation and direction, as well as OSI and DSI were calculated using Fourier-interpolated tuning curves. Pearson's correlation coefficient was used to obtain pair-wise response correlations, either from average responses to the stimulus (signal correlation) or from mean-subtracted responses (noise correlation). Small volumes of fluorescent microspheres were injected into the imaged region to facilitate identification of the region in the sliced brain. Coronal slices were cut after dissection of the brain, and whole-cell recordings from up to four cells simultaneously were carried out in the vicinity of the microsphere tract (identified by two-photon microscopy). The presence of synaptic connections was tested by evoking five spikes at 30 Hz in each cell, repeated 30–90 times. Connection probability is the number of detected connections over the total number of potential connections assayed. Probability of finding uni- or bidirectionally connected pairs was calculated as the number of uni- or bidirectionally connected pairs over the total number of pairs. To register *in vivo* and *in vitro* image stacks and to match the same neurons imaged *in vivo* and recorded from *in vitro*, three-dimensional image registration by affine transformation using custom-written MATLAB software was performed subsequent to the experiment. To relate connectivity to functional properties, the asymptotic Cochran–Armitage test for trend was used to test for significance.

Full Methods and any associated references are available in the online version of the paper at www.nature.com/nature.

Received 8 September 2010; accepted 1 February 2011.
Published online 10 April 2011.

1. Bosking, W. H., Zhang, Y., Schofield, B. & Fitzpatrick, D. Orientation selectivity and the arrangement of horizontal connections in tree shrew striate cortex. *J. Neurosci.* **17,** 2112–2127 (1997).
2. Gilbert, C. D. & Wiesel, T. N. Columnar specificity of intrinsic horizontal and corticocortical connections in cat visual cortex. *J. Neurosci.* **9,** 2432–2442 (1989).
3. Roerig, B. & Kao, J. P. Organization of intracortical circuits in relation to direction preference maps in ferret visual cortex. *J. Neurosci.* **19,** RC44 (1999).
4. Weliky, M., Kandler, K., Fitzpatrick, D. & Katz, L. C. Patterns of excitation and inhibition evoked by horizontal connections in visual cortex share a common relationship to orientation columns. *Neuron* **15,** 541–552 (1995).
5. Song, S., Sjöström, P. J., Reigl, M., Nelson, S. & Chklovskii, D. B. Highly nonrandom features of synaptic connectivity in local cortical circuits. *PLoS Biol.* **3,** e68 (2005).
6. Yoshimura, Y., Dantzker, J. L. M. & Callaway, E. M. Excitatory cortical neurons form fine-scale functional networks. *Nature* **433,** 868–873 (2005).
7. Yoshimura, Y. & Callaway, E. M. Fine-scale specificity of cortical networks depends on inhibitory cell type and connectivity. *Nature Neurosci.* **8,** 1552–1559 (2005).
8. Brown, S. P. & Hestrin, S. Intracortical circuits of pyramidal neurons reflect their long-range axonal targets. *Nature* **457,** 1133–1136 (2009).
9. Thomson, A. M., Bannister, A. P., Mercer, A. & Morris, O. T. Target and temporal pattern selection at neocortical synapses. *Phil. Trans. R. Soc. Lond. B* **357,** 1781–1791 (2002).
10. Holmgren, C., Harkany, T., Svennenfors, B. & Zilberter, Y. Pyramidal cell communication within local networks in layer 2/3 of rat neocortex. *J. Physiol. (Lond.)* **551,** 139–153 (2003).
11. Mrsic-Flogel, T. D. *et al.* Homeostatic regulation of eye-specific responses in visual cortex during ocular dominance plasticity. *Neuron* **54,** 961–972 (2007).
12. Ohki, K., Chung, S., Ch'ng, Y. H., Kara, P. & Reid, R. C. Functional imaging with cellular resolution reveals precise micro-architecture in visual cortex. *Nature* **433,** 597–603 (2005).
13. Nimmerjahn, A., Kirchhoff, F., Kerr, J. N. D. & Helmchen, F. Sulforhodamine 101 as a specific marker of astroglia in the neocortex *in vivo*. *Nature Methods* **1,** 31–37 (2004).
14. Denk, W., Strickler, J. H. & Webb, W. W. Two-photon laser scanning fluorescence microscopy. *Science* **248,** 73–76 (1990).
15. Stosiek, C., Garaschuk, O., Holthoff, K. & Konnerth, A. *In vivo* two-photon calcium imaging of neuronal networks. *Proc. Natl Acad. Sci. USA* **100,** 7319–7324 (2003).
16. Jia, H., Rochefort, N. L., Chen, X. & Konnerth, A. Dendritic organization of sensory input to cortical neurons *in vivo*. *Nature* **464,** 1307–1312 (2010).
17. Alonso, J. M. & Martinez, L. M. Functional connectivity between simple cells and complex cells in cat striate cortex. *Nature Neurosci.* **1,** 395–403 (1998).
18. Kohn, A. & Smith, M. A. Stimulus dependence of neuronal correlation in primary visual cortex of the macaque. *J. Neurosci.* **25,** 3661–3673 (2005).
19. Aertsen, A. M., Gerstein, G. L., Habib, M. K. & Palm, G. Dynamics of neuronal firing correlation: modulation of "effective connectivity". *J. Neurophysiol.* **61,** 900–917 (1989).
20. Mariño, J. *et al.* Invariant computations in local cortical networks with balanced excitation and inhibition. *Nature Neurosci.* **8,** 194–201 (2005).
21. Ben-Yishai, R., Bar-Or, R. L. & Sompolinsky, H. Theory of orientation tuning in visual cortex. *Proc. Natl Acad. Sci. USA* **92,** 3844–3848 (1995).
22. Douglas, R. J., Koch, C., Mahowald, M., Martin, K. A. & Suarez, H. H. Recurrent excitation in neocortical circuits. *Science* **269,** 981–985 (1995).
23. Li, W., Piëch, V. & Gilbert, C. D. Contour saliency in primary visual cortex. *Neuron* **50,** 951–962 (2006).
24. Alonso, J. M., Usrey, W. M. & Reid, R. C. Rules of connectivity between geniculate cells and simple cells in cat primary visual cortex. *J. Neurosci.* **21,** 4002–4015 (2001).
25. Clopath, C., Büsing, L., Vasilaki, E. & Gerstner, W. Connectivity reflects coding: a model of voltage-based STDP with homeostasis. *Nature Neurosci.* **13,** 344–352 (2010).
26. Tolhurst, D. J., Movshon, J. A. & Dean, A. F. The statistical reliability of signals in single neurons in cat and monkey visual cortex. *Vision Res.* **23,** 775–785 (1983).
27. Barlow, H. Redundancy reduction revisited. *Network* **12,** 241–253 (2001).
28. Alitto, H. J. & Dan, Y. Function of inhibition in visual cortical processing. *Curr. Opin. Neurobiol.* **20,** 340–346 (2010).
29. Marshel, J. H., Mori, T., Nielsen, K. J. & Callaway, E. M. Targeting single neuronal networks for gene expression and cell labeling *in vivo*. *Neuron* **67,** 562–574 (2010).

30. Denk, W. & Horstmann, H. Serial block-face scanning electron microscopy to reconstruct three-dimensional tissue nanostructure. *PLoS Biol.* **2,** e329 (2004).

Supplementary Information is linked to the online version of the paper at www.nature.com/nature.

Acknowledgements We thank T. Margrie for discussions about the project and the manuscript, and J. Vogelstein for the spike inference algorithm. This work was supported by the Wellcome Trust (T.D.M.-F.), the European Research Council (T.D.M.-F.), the European Molecular Biology Organisation (S.B.H.), the Medical Research Council and FP7 grant #243914 (K.A.B., P.J.S.), the Overseas Research Students Award Scheme and UCL studentship (H.K.).

Author Contributions H.K. and S.B.H. performed experiments and data analysis. H.K. developed image registration software using preliminary data obtained by S.B.H. and K.A.B., and programs for data analysis. B.P. developed image acquisition software and the program for extracting calcium transients. P.J.S. designed electrophysiology setup and software for acquisition and analysis. B.P., H.K., S.B.H. and T.D.M.-F. built experimental setups. H.K. and T.D.M.-F. wrote the paper.

Author Information Reprints and permissions information is available at www.nature.com/reprints. The authors declare no competing financial interests. Readers are welcome to comment on the online version of this article at www.nature.com/nature. Correspondence and requests for materials should be addressed to T.D.M.-F. (t.mrsic-flogel@ucl.ac.uk).

METHODS

Animals and surgical procedures. All experimental procedures were carried out in accordance with institutional animal welfare guidelines and were licensed by the UK Home Office. Experiments were performed on C57Bl/6 mice between postnatal day 22–26, when both intrinsic and visually driven cortical responses exhibit a relatively mature phenotype[31,32]. Mice were initially anaesthetized with a mixture of Fentanyl (0.05 mg kg^{-1}), Midazolam (5.0 mg kg^{-1}), and Medetomidin (0.5 mg kg^{-1}). Light anaesthesia was maintained during recordings by isoflurane (0.3–0.5%) in a 60:40% mixture of O_2:N_2O delivered via a small nose cone. Surgery was performed as described previously[11]. Briefly, a small craniotomy (1–2 mm) was carried out over primary visual cortex and sealed after dye injection with 1.6% agarose in HEPES-buffered artificial cerebrospinal fluid (ACSF) and a cover slip.

Dye loading and two-photon calcium imaging *in vivo*. For bulk loading of cortical neurons, the calcium-sensitive dye Oregon Green Bapta-1 AM (OGB-1 AM; Molecular Probes) was first dissolved in 4 µl DMSO containing 20% Pluronic F-127 (Molecular Probes), and further diluted (1/11) in dye buffer (150 mM NaCl, 2.5 mM KCl and 10 mM HEPES (pH 7.4)) to yield a final concentration of 0.9 mM. Sulphorhodamine 101 (SR101, 50 µM; Molecular Probes) was added to the solution to distinguish astrocytes from neurons[13]. The dye was slowly pressure-injected into the right visual cortex at a depth of 150–200 µm with a micropipette (3–5 MΩ, 3–10 psi, 2–4 min) under visual control by two-photon imaging (×10 water immersion objective, Olympus). Activity of cortical neurons was monitored by imaging fluorescence changes with a custom-built microscope and a mode-locked Ti:sapphire laser (Mai Tai, Spectra-Physics) at 830 nm through a ×40 water immersion objective (0.8 NA, Olympus). Scanning and image acquisition were controlled by custom software written in LabVIEW (National Instruments). The average laser power delivered to the brain was <50 mW.

Imaging frames of 256 × 256 pixels were acquired at 7.6 Hz, starting at ~110 µm below cortical surface, corresponding to superficial layer 2 in mouse V1. After each recording, the focal plane and imaging position was checked and realigned with the initial image if necessary. To obtain visually evoked responses from all neurons in a cortical volume of approximately 285 × 285 × 60–120 µm^3, images were recorded at 9 to 18 cortical depths with a spacing of 7 µm. At the end of each experiment, fluorescent microspheres (Lumafluor) were carefully pressure-injected into the imaged volume with a glass pipette, resulting in small fluorescent landmarks (5–20 µm diameter) along the pipette track. These landmarks were used to assist in subsequent identification of the imaged region in the sliced brain (see later), as well as fine-scale registration of *in vivo* and *in vitro* image stacks.

Visual stimulation. Visual stimuli were generated using MATLAB Psychophysics Toolbox[33,34], and displayed on an LCD monitor (60 Hz refresh rate) positioned 20 cm from the left eye, roughly at 45 degrees to the long axis of the animal, covering ~105 × 85 degrees of visual space. At the beginning of each experiment, the appropriate retinotopic position in visual cortex was determined using small grating stimuli at 12–24 neighbouring positions. Only cortical regions in the monocular part of primary visual cortex were included in the analysis. The monitor was repositioned such that the preferred retinotopic position of most imaged neurons was roughly in the middle of the monitor. Calcium signals were measured in response to sequences of full-field grating stimuli and natural movies. Square-wave gratings (0.035 cycles per degree, 2 cycles s^{-1}, 100% contrast) drifting in eight different directions were randomly interleaved, with the grating standing for 1.4–1.9 s before moving for 0.9–1.5 s (six repetitions per grating). Naturalistic movies consisted of 30 or 40 s sequences of moving scenes compiled from David Attenborough's Life of Mammals (BBC) and cage scenes from a head-mounted mouse camera, adjusted to 70% mean contrast (repeated 4–7 times).

Analysis of calcium signals. Image sequences were aligned for tangential drift and analysed with custom programs written in ImageJ (NIH), MATLAB (Mathworks) and LabVIEW. Recordings with significant brain movements, vertical drift, or both were excluded from further analysis. Outlines of neurons recorded were semi-automatically defined using software written in MATLAB (Mathworks). All pixels within each ROI were averaged to give a single time course ($\Delta F/F$), which was additionally high-pass filtered at a cut-off frequency of 0.02 Hz to remove slow fluctuations in the signal.

Spike trains were inferred from calcium signals using a fast non-negative deconvolution method that approximates the maximum a posteriori spike train for each neuron, given the fluorescence observations[35]. Performance of the algorithm was tested by cell-attached recordings performed simultaneously with calcium imaging. There was a close correspondence between inferred and recorded spike rates (mean correlation ± s.d. = 0.82 ± 0.06; nine cells from four animals).

Visual responsiveness was determined by the following procedure. For all stimulus repetitions, inferred spike trains were moving-average filtered with a time window of three frames (~0.394 s). The smoothed firing rates at corresponding points of the stimulus were then treated as groups and tested for differences by one-way ANOVA. Neurons with a P value less than 0.05 were considered visually responsive. This allowed neurons that exhibited consistent elevated firing during at least one period of stimulus presentation to be detected. Among cells responsive to grating stimuli, the sum of firing rates of eight frames (~1.05 s) 0.13 s after the onset of grating drift was taken as the response to each stimulus. Responses from different trials were averaged to obtain the orientation tuning curve. This orientation tuning curve was then Fourier interpolated to 360 points, and the preferred direction was determined by the angle at which the interpolated tuning curve attained its maximum. The preferred orientation was taken as the modulus of the preferred direction to 180 degrees. OSI was calculated as $(R_{best} - R_{ortho})/(R_{best} + R_{ortho})$, where R_{best} is the interpolated response to the best direction, and R_{ortho} is the average of interpolated responses to the directions orthogonal to best responding direction. DSI was calculated as $1 - R_{null}/R_{best}$, where R_{null} is the interpolated response to the angle opposite the best responding direction. When relating connection probability to orientation selectivity or direction selectivity, neurons were defined to be orientation selective if OSI >0.4, and direction selective if DSI >0.3. Varying these criteria from 0.2 to 0.6 did not change the results (Supplementary Fig. 3). We used Pearson's correlation coefficient to obtain pair-wise response correlations for cell pairs, using estimated spike rates. Signal correlation was calculated as the correlation coefficient of the average responses to stimulus. Noise correlation was found by subtracting the average response from the responses to each trail, and then calculating the correlation coefficient of mean-subtracted responses.

***In vitro* whole-cell recording.** We carried out imaging experiments on a total of 16 mice that were followed by patch-clamp recordings *in vitro*. After the functional properties of individual neurons had been determined *in vivo* by two-photon calcium imaging, the mouse brain was rapidly removed and dissected in ice-cold ACSF containing 125 mM NaCl, 2.5 mM KCl, 1 mM $MgCl_2$, 1.25 mM NaH_2PO_4, 2 mM $CaCl_2$, 26 mM $NaHCO_3$, 25 mM dextrose; osmolarity 315–325 mOsm, bubbled with 95% O_2/5% CO_2, pH 7.4. Visual cortex slices (300 µm) were cut coronally (HM 650 V Vibration Microtome, MICROM) and were incubated at 34 °C for thirty minutes before they were transferred to the recording chamber. The slice containing the imaged region was identified by the presence of OGB-1 green fluorescence and the red microsphere injection site. To reveal the relative locations of cells, a detailed morphological stack of the slice was acquired with a custom-built microscope and a mode-locked Ti:sapphire laser (Chameleon, Coherent) at 830 nm through a ×16 water immersion objective (0.8 NA, Nikon). Scanning and image acquisition were controlled by custom software written in LabVIEW. Whole-cell recordings from up to four cells were carried out in regions identified by visually comparing image stacks obtained *in vivo* and *in vitro*, using red fluorescent microspheres and the pial surface as reference. At this point, the experimenter was blind to the functional identity of the recorded neurons. Recordings were carried out in 28 °C ACSF, using Multiclamp 700B amplifiers (Axon Instruments) and data were acquired using custom software[36] running in Igor Pro (WaveMetrics). Recording pipettes were filled with internal solution containing 5 mM KCl, 115 mM K-gluconate, 10 mM K-HEPES, 4 mM MgATP, 0.3 mM NaGTP, 10 mM Na-phosphocreatine, 0.1% w/v biocytin, 40 µM Alexa Fluor 594; osmolarity 290–295 mOsm, pH 7.2. The chloride reversal potential was approximately −85.2 mV. Junction potential was not corrected for. Cells were approached under visual guidance using laser-scanning Dodt contrast imaging. After break-through, the presence of synaptic connections was tested using five suprathreshold 5-ms-long current pulses delivered as 30-Hz trains into each cell sequentially while monitoring for postsynaptic responses in the other cells, repeated at least 30 times at 15-s intervals. Postsynaptic traces were averaged, and monosynaptic excitatory connections were deemed present when there were action-potential-locked depolarizing postsynaptic potentials associated with all five presynaptic spikes that exhibited millisecond latency[37]. Latency was measured as the time between the peak of the action potential and 5% of the EPSP. If no spike-locked depolarizing postsynaptic potentials was present, up to 60 additional repetitions were acquired to ensure the absence of a postsynaptic response. With this approach, unitary EPSPs as small as 0.015 mV have been reported previously[5], the smallest EPSP in the present data set was 0.035 mV. PPR was calculated as the amplitude of the second evoked EPSP over that of the first one. Input resistance was monitored throughout recordings by measuring the steady-state membrane potential change due to brief −25 pA current injections. After connectivity mapping, step currents from −50 pA to 700 pA were injected at 50 pA increments and spike threshold was measured from the inflexion point of the minimally suprathreshold trace. Spike height was the difference between spike threshold and peak. Spike half-width was measured at the mean of threshold and peak. Pyramidal neurons were identified according to morphology in Alexa 594 filled image stacks (Fig. 2a), electrophysiological properties (resting membrane potential approximately −80 mV, spike half-width >1 ms, spike height ~80 mV, regular spiking pattern typical of pyramidal neurons with current injection, see Supplementary Fig. 2c–e) and, in the presence of connections, depolarizing postsynaptic potentials (Figs 2c, 3b).

Registration of *in vivo* and *in vitro* image stacks. To accurately match up *in vivo* and *in vitro* image stacks and to locate neurons of known *in vivo* functional preference, three-dimensional image registration using custom-written MATLAB software was performed after patch-clamp experiments. The two stacks containing the same region to be matched differ in rotation and translation, as well as scales along axes. In other words, taking the centre of each stack as origin, the same points in the two stacks can be related by affine transformation. This can be written as

$$\mathbf{y} = \mathbf{A}\mathbf{x} + \mathbf{b}$$

Where $\mathbf{x}$ and $\mathbf{y}$ are column vectors of coordinates in *in vivo* and *in vitro* stack, respectively, $\mathbf{A}$ is a 3×3 matrix representing linear transformation, and $\mathbf{b}$ is the translation. To find the affine transformation four pairs of corresponding points, $(\mathbf{x}_i,\mathbf{y}_i)$, where $i = 1, 2, 3, 4$, were manually picked from the stacks, using landmarks such as blood vessel bifurcations, fluorescent bead injections, cortical surface, and/or brightly labelled astrocytes. The relationship between the first pair of points $(\mathbf{x}_1,\mathbf{y}_1)$ is

$$\mathbf{y}_1 = \mathbf{A}\mathbf{x}_1 + \mathbf{b}$$

$$\mathbf{b} = \mathbf{y}_1 - \mathbf{A}\mathbf{x}_1$$

Substitute this into

$$\mathbf{A}[\,\mathbf{x}_2 \quad \mathbf{x}_3 \quad \mathbf{x}_4\,] + [\,\mathbf{b} \quad \mathbf{b} \quad \mathbf{b}\,] = [\,\mathbf{y}_2 \quad \mathbf{y}_3 \quad \mathbf{y}_4\,]$$

and let $\mathbf{x}'_i = \mathbf{x}_i - \mathbf{x}_1$, $\mathbf{y}'_i = \mathbf{y}_i - \mathbf{y}_1$, where $i = 2, 3, 4$, gives

$$\mathbf{A}([\,\mathbf{x}_2 \quad \mathbf{x}_3 \quad \mathbf{x}_4\,] - [\,\mathbf{x}_1 \quad \mathbf{x}_1 \quad \mathbf{x}_1\,]) = [\,\mathbf{y}_2 \quad \mathbf{y}_3 \quad \mathbf{y}_4\,] - [\,\mathbf{y}_1 \quad \mathbf{y}_1 \quad \mathbf{y}_1\,]$$

$$\mathbf{A}[\,\mathbf{x}'_2 \quad \mathbf{x}'_3 \quad \mathbf{x}'_4\,] = [\,\mathbf{y}'_2 \quad \mathbf{y}'_3 \quad \mathbf{y}'_4\,]$$

$$\mathbf{A} = [\,\mathbf{y}'_2 \quad \mathbf{y}'_3 \quad \mathbf{y}'_4\,][\,\mathbf{x}'_2 \quad \mathbf{x}'_3 \quad \mathbf{x}'_4\,]^{-1}$$

Knowing the linear transformation $\mathbf{A}$, $\mathbf{b}$ can also be found.

In practice, to assist the process of identifying corresponding points, after picking three pairs of points, the image stacks were both rotated such that the planes containing the three pairs of points became parallel to the *x*–*y* plane, and the *in vitro* stack was further transformed such that the stacks became roughly registered in two dimensions on the planes but not along the *z*-axis (Supplementary Fig. 1a, b). To do this, let $\mathbf{R}_v$ and $\mathbf{R}_t$ be the matrices for rotating *in vivo* and *in vitro* stacks respectively, and let $\mathbf{u} = [\,u_x \quad u_y \quad u_z\,]^T$ be a unit vector, the matrix for rotating a point around $\mathbf{u}$ by angle θ (right handedly) is given by

$$\mathbf{R} = \begin{bmatrix} 0 & -u_z & u_y \\ u_z & 0 & -u_x \\ -u_y & u_x & 0 \end{bmatrix} \sin\theta + (\mathbf{I} - \mathbf{u}\mathbf{u}^T)\cos\theta + \mathbf{u}\mathbf{u}^T$$

where $\mathbf{I}$ is the identity matrix. To rotate the *in vivo* stack such that the plane containing the first three points picked becomes parallel to the *x*–*y* plane, the vector and the angle are

$$\mathbf{u}_v = \frac{(\mathbf{x}'_2 \times \mathbf{x}'_3) \times \mathbf{e}_z}{\|(\mathbf{x}'_2 \times \mathbf{x}'_3) \times \mathbf{e}_z\|}$$

$$\theta_v = \cos^{-1}\left(\frac{(\mathbf{x}'_2 \times \mathbf{x}'_3)\cdot\mathbf{e}_z}{\|\mathbf{x}'_2 \times \mathbf{x}'_3\|}\right)$$

where $\mathbf{e}_z = [\,0 \quad 0 \quad 1\,]^T$, $\times$ denotes cross product, $\cdot$ denotes dot product and $\|\|$ denotes norm. Substituting these into the formula for rotation matrix above, we can find $\mathbf{R}_v$, and similarly $\mathbf{R}_t$ can also be found. To register the two planes in two dimensions, a further linear transformation parallel to the *x*–*y* plane can be applied to the *in vitro* stack. Let $\mathbf{x}'_{iR}$ be the *x*, *y* components of $\mathbf{R}_v\mathbf{x}'_i$, and $\mathbf{y}'_{iR}$ be the *x*, *y* components of $\mathbf{R}_t\mathbf{y}'_i$, where $i = 2, 3$, the matrix $\mathbf{M}$ needed for the two-dimensional transformation is given by

$$\mathbf{M}[\,\mathbf{y}'_{2R} \quad \mathbf{y}'_{3R}\,] = [\,\mathbf{x}'_{2R} \quad \mathbf{x}'_{3R}\,]$$

$$\mathbf{M} = [\,\mathbf{x}'_{2R} \quad \mathbf{x}'_{3R}\,][\,\mathbf{y}'_{2R} \quad \mathbf{y}'_{3R}\,]^{-1}$$

Therefore, the transformation $\mathbf{T}_t$ applied to the *in vitro* stack is

$$\mathbf{T}_t = \begin{bmatrix} \mathbf{M} & 0 \\ 0 & 1 \end{bmatrix} \mathbf{R}_t$$

After this step, we picked one more pair of corresponding points from a plane different from the plane that contained the initial three pairs of points (Supplementary Fig. 1b, lower panel), which is necessary for $[\,\mathbf{x}'_2 \quad \mathbf{x}'_3 \quad \mathbf{x}'_4\,]$ and $[\,\mathbf{y}'_2 \quad \mathbf{y}'_3 \quad \mathbf{y}'_4\,]$ to be invertible, $\mathbf{A}$ can then be found and applied to the *in vivo* stack. With the affine transformation known, we could find the correspondence between points. When rotating or transforming the image stacks, trilinear interpolation was used to assign pixel values. After registration, we inspected several planes of the transformed stack containing neurons recorded *in vitro* and made use of three-dimensional relationships of nearby cells to visually verify the matching (compare Fig. 1g, h and Supplementary Fig. 1c). Among 126 pyramidal neurons patched, matching was successful for 116 while 10 failed: 3 cells were occluded in the *in vivo* stack by a blood vessel, and 7 cells did not show convincing matching in three dimensions on visual inspection.

Analysis of connection probabilities. Connection probabilities were calculated as the number of connections detected over the number of potential connections assayed. For example, with one quadruplet there are $4 \times 3 = 12$ potential connections, and if two connections were detected the corresponding figure would be 2/12. Probabilities of unidirectional and bidirectional connections were calculated as the number of unidirectionally and bidirectionally connected pairs over the total number of pairs, respectively. To relate connectivity to functional properties, the asymptotic Cochran–Armitage test for trend was used to test for significance[38]. Scores of [2, 1, 0] and [2, 1, 0, 1, 2] were used in the test to relate connection probability or probability of finding bidirectionally connected pairs to increase in ΔOri among orientation selective pairs and direction selective pairs, respectively. Scores of [0, 1, 2, 3, 4] were used to relate connection probability or probability of finding bidirectionally connected pairs to the increase in signal correlation. To relate connection probability to increase in noise correlation, scores of [0, 1, 2] were used.

Criteria for inclusion in data analysis. After patching, image stacks of patched neurons filled with Alexa 594 were taken and coordinates of approximate centres of neuronal somata were manually picked in a custom-written MATLAB program. The distance between the slice surface right above the patched neuron and the soma centre was taken as the depth of neuron from the slice surface. Only neuronal pairs in which both neurons were located at >60 μm depth and with an inter-soma distance of <50 μm were included in the analysis relating connectivity to visual functional properties. On average we patched 7.9 neurons (range: 2–14) and assayed 13.9 potential connections (range: 2–31) per slice for neuronal pairs located deeper than 60 μm in the slice and separated by less than 50 μm.

Neuronal pairs closer to the slice surface are more likely to have connections severed, and we found a significant increase in the probability of finding connections with the depth of the potential presynaptic neuron ($P = 0.043$, Cochran–Armitage test) or postsynaptic neuron ($P = 0.041$, Cochran–Armitage test) (Supplementary Fig. 6a, b). However, inclusion of cell pairs closer to the slice surface (which increases the false-negative rate of connection detection), or increasing the depth criteria (which reduces sample size) in analysis did not change the main findings (Supplementary Fig. 6d–f). Between neuronal pairs located deeper than 60 μm from the slice surface, 222 connections were assayed between pairs separated by less than 50 μm. We did not find a significant difference in connection probability for neuronal pairs separated by less than 25 μm compared to those spaced farther apart ($P = 0.594$, chi-squared test; Supplementary Fig. 6c).

In 18 out of 113 pairs, high-quality recording was achieved in one cell only (for example, the other cell was very depolarized/unhealthy, or the seal resistance was less than 1 GΩ). As action potentials could still be evoked in both neurons, these pairs were included as pairs in which connectivity was assayed in the direction from the unhealthy cell to the healthy cell only. Data from these pairs were included in the analysis of connection probability, but not in the analysis of probability of finding bidirectional or unidirectional pairs. Analysis of intrinsic electrophysiological properties was carried out only if series resistance was less than 30 MΩ.

31. Smith, S. L. & Trachtenberg, J. T. Experience-dependent binocular competition in the visual cortex begins at eye opening. *Nature Neurosci.* **10,** 370–375 (2007).
32. Rochefort, N. L. *et al.* Sparsification of neuronal activity in the visual cortex at eye-opening. *Proc. Natl Acad. Sci. USA* **106,** 15049–15054 (2009).
33. Brainard, D. H. The Psychophysics Toolbox. *Spat. Vis.* **10,** 433–436 (1997).
34. Pelli, D. G. The VideoToolbox software for visual psychophysics: transforming numbers into movies. *Spat. Vis.* **10,** 437–442 (1997).
35. Vogelstein, J. T. *et al.* Fast non-negative deconvolution for spike train inference from population calcium imaging. *J. Neurophysiol.* (2010).
36. Sjöström, P. J., Turrigiano, G. G. & Nelson, S. B. Rate, timing, and cooperativity jointly determine cortical synaptic plasticity. *Neuron* **32,** 1149–1164 (2001).
37. Debanne, D. *et al.* Paired-recordings from synaptically coupled cortical and hippocampal neurons in acute and cultured brain slices. *Nature Protocols* **3,** 1559–1568 (2008).
38. Agresti, A. *Categorical Data Analysis* 2nd edn (Wiley InterScience, 2002).